

Two-body interaction induced phase transitions and intermediate phases in nonreciprocal non-Hermitian quasicrystals

Yalun Zhang¹ and Longwen Zhou^{1,2,3,4,*}

¹*College of Physics and Optoelectronic Engineering,
Ocean University of China, Qingdao 266100, China*

²*Institute of Theoretical Physics, Chinese Academy of Sciences, Beijing 100190, China*

³*Key Laboratory of Optics and Optoelectronics, Qingdao 266100, China*

⁴*Engineering Research Center of Advanced Marine Physical Instruments and Equipment of MOE, Qingdao 266100, China*

(Dated: 2025-03-04)

Non-Hermitian phenomena, such as exceptional points, non-Hermitian skin effects, and topologically nontrivial phases have attracted continued attention. In this work, we reveal how interactions and nonreciprocal hopping could collectively influence the behavior of two interacting bosons on quasiperiodic lattices. Focusing on the Bose-Hubbard model with Aubry-André-Harper quasiperiodic modulations and hopping asymmetry, we discover that interactions could enlarge the localization transition point of the noninteracting system into an intermediate mobility edge phase, in which localized doublons formed by bosonic pairs can coexist with delocalized states. Under the open boundary condition, the bosonic doublons could further show non-Hermitian skin effects, realizing doublon condensation at the edges, and their direction of skin-localization can be flexibly tuned by the hopping parameters. A framework is developed to characterize the spectral, localization, and topological transitions accompanying these phenomena. Our work advances the understanding of localization and topological phases in non-Hermitian systems, particularly in relation to multiparticle interactions.

I. INTRODUCTION

Anderson localization (AL) refers to the absence of diffusion in disordered media [1–3]. As a generic phenomenon, it plays an important role in both classical and quantum transport of waves under spatial randomness [4]. In quantum regime, it also describes a class of metal-insulator phase transition driven by disorder [5, 6]. Over the past six decades, the AL has attracted continued interest in both theoretical [7–13] and experimental [14–19] studies. However, the fate of localization in open systems and under many-body interactions is still a challenging issue that has not been fully resolved.

Non-Hermitian systems, usually characterized by non-Hermitian Hamiltonians constitute ideal setups to explore the interplay among localization, environmental effects and interactions. In recent years, non-Hermitian systems have attracted increasing attention due to their distinctive physics, such as the parity-time-reversal (PT) transitions [20–22], exceptional points [23–28], non-Hermitian skin effects (NHSEs) [29–33] and enriched symmetry classifications of topological phases [34–40]. Meanwhile, the interplay between disorder and non-Hermitian effects may lead to unique types of spectral, localization, topological and entanglement transitions [41–74], yielding universality classes of localization beyond closed-system contexts [75–78]. With additional elements like lattice dimerization, long-range hopping, non-Abelian potential and time-period driving, intermediate phases and mobility edges could also emerge in disor-

dered non-Hermitian systems even in one spatial dimension [79–96], enriching further the non-Hermitian localization phenomenon.

Interaction could greatly complicate the AL in non-Hermitian systems due to its active competition with other localization mechanisms, including random or correlated disorder and NHSEs. Great efforts have been made towards the understanding of “many-body localization” in non-Hermitian settings, with a focus on multiple interacting particles in lattices of relatively small sizes [97–107]. Nevertheless, considering a few interacting particles in relatively large lattices may offer necessary insights regarding how interactions could drive different phase transitions and criticality in the thermodynamic limit (with system size $L \rightarrow \infty$) [108–116]. Motivated by these considerations, we explore in this work the interaction-driven phase transitions and intermediate mobility edge phases in non-Hermitian quasicrystals (NHQCs). Focusing on two interacting bosons in one-dimensional (1D) Aubry-André-Harper (AAH) lattices with quasiperiodic onsite potentials and nonreciprocal hoppings, we reveal that the interactions could not only transform the AL critical points of noninteracting systems into intermediate mobility edge phases with coexisting extended and localized states, but also push the boundaries of fully localized phases towards stronger asymmetric hopping regions. Within an intermediate phase, extended two-boson states can coexist with bounded boson pairs forming doublons, which could also subject to NHSEs under the open boundary condition (OBC). The borders between extended, intermediate and localized phases are further found to carry topologically nontrivial signatures.

The rest of the paper is organized as follows. In Sec. II,

* zhoulw13@u.nus.edu

we introduce the model considered in this work, summarizing its known features in the noninteracting limit, and presenting the methods we take to study its physical properties. In Sec. III, we characterize the real-complex spectra transitions, localization transitions, topological transitions and intermediate mobility edge phases in representative NHQCs with asymmetric hoppings, tracing their origins back to the interplay between interactions and non-Hermitian effects of two interacting bosons. In Sec. IV, we focus on the strong-interaction regime and explore the competition of two different localization mechanisms (disorder vs NHSEs) on bosonic doublons. In Sec. V, we summarize our results and discuss potential future directions.

II. MODEL AND METHODS

This section introduces the NHQC model that we will consider in this work. Without interactions, features of the model regarding its spectral, localization and topological transitions will be recapped. With onsite Bose-Hubbard interactions, we introduce quantities to characterize the phases and transitions in our system, including the ratio of complex energies, inverse participation ratios (IPRs) and topological winding numbers.

A. Model

In this work, we investigate phases and transitions caused by the collaboration among quasiperiodic disorder, non-Hermitian asymmetric couplings and interparticle interactions in one dimension. A minimal model that takes into account all these competing factors can be described by the tight-binding Hamiltonian

$$\hat{H} = \sum_l \left(J_L \hat{b}_l^\dagger \hat{b}_{l+1} + J_R \hat{b}_{l+1}^\dagger \hat{b}_l \right) + \sum_l \left[2V \cos(2\pi\alpha l) \hat{n}_l + \frac{U}{2} \hat{n}_l (\hat{n}_l - 1) \right]. \quad (1)$$

A schematic diagram of the model is shown in Fig. 1(a). \hat{b}_l^\dagger (\hat{b}_l) creates (annihilates) a boson on the lattice site $l \in \mathbb{Z}$. $\hat{n}_l = \hat{b}_l^\dagger \hat{b}_l$ is the particle number operator on the l th site. J_L and J_R are right-to-left and left-to-right nearest-neighbor hopping amplitudes, respectively, which are asymmetric so long as $J_L^* \neq J_R$. Without loss of generality, we will only consider cases with $J_L, J_R \geq 0$. The Hamiltonian \hat{H} is then non-Hermitian ($\hat{H} \neq \hat{H}^\dagger$) if $J_L \neq J_R$. $V \in \mathbb{R}$ controls the strength of onsite potential. The latter is quasiperiodic when α is irrational. Throughout the calculations, we choose α to be the inverse golden ratio $\frac{\sqrt{5}-1}{2}$. Taking other irrational values for α yields consistent results. Finally, U is the strength of onsite Bose-Hubbard interactions, i.e., the interaction energy of two bosons on the same lattice site.

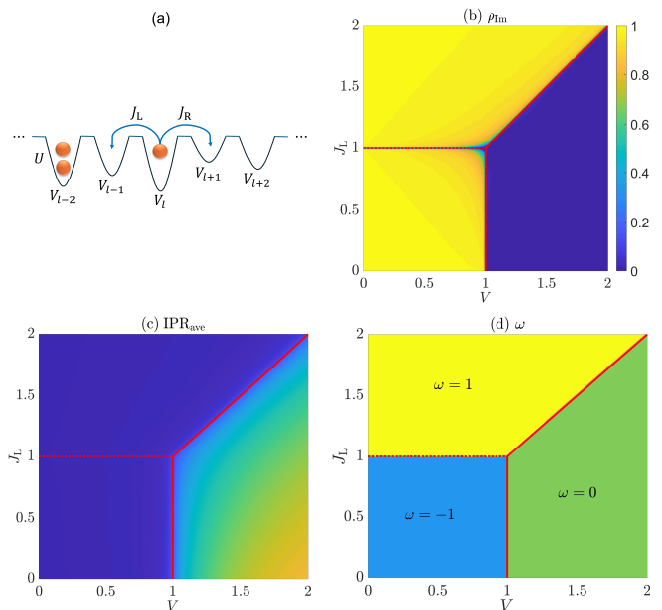


FIG. 1. A sketch of the model [in (a)] and its single-particle phases described by different variables [in (b)–(d), with $U = 0$] under the PBC. In (a), we have $V_l \equiv 2V \cos(2\pi\alpha l)$, which is quasiperiodic in l for any irrational α . (b) shows the ratio of eigenenergies of \hat{H}_0 with nonzero imaginary parts ρ_{Im} [Eq. (3)] vs (V, J_L) . (c) shows the averaged IPRs [Eq. (5)] over all eigenstates of \hat{H}_0 vs (V, J_L) . (b) and (c) share the same color bar. (d) gives the topological phase diagram characterized by the winding number ω [Eq. (6)]. In (b)–(d), the solid line denotes the boundary [Eq. (2)] of PT, localization and topological transitions under the PBC, while the dotted line represents the boundary ($J_L = J_R$ and $J_L, J_R < V$) between left and right skin-localizations of bulk states under the OBC. The hopping amplitude $J_R = 1$ and the length of lattice $L = 89$ are set to be the same for (b)–(d).

Without interactions, the system described by Eq. (1) reduces to the quasiperiodic nonreciprocal AAH model, whose properties has been investigated [49, 62]. Let us denote the noninteracting part of \hat{H} by $\hat{H}_0 \equiv \hat{H}(U = 0)$. Under the periodic boundary condition (PBC), a three-fold transition was identified at

$$|V| = \max(J_L, J_R). \quad (2)$$

When $|V| < \max(J_L, J_R)$, the spectrum of \hat{H}_0 is complex and all its eigenstates are spatially extended. When $|V| > \max(J_L, J_R)$, the spectrum of \hat{H}_0 becomes real and all its eigenstates are exponentially localized. Moreover, a spectral winding number ω can be defined for \hat{H}_0 , whose value is $\omega = \pm 1$ ($\omega = 0$) when \hat{H}_0 holds a complex (real) spectrum. Therefore, at the triple criticality [Eq. (2)] of the noninteracting \hat{H}_0 , we encounter a PT transition in the spectrum, a localization transition of the eigenstates, plus a topological transition accompanied by the unit jump of winding number ω . Meanwhile, the system described by \hat{H}_0 has NHSEs under OBC due

to the hopping asymmetry when $J_L \neq J_R$. Interestingly, the winding number ω takes the value -1 ($+1$) when $J_L < J_R$ ($J_L > J_R$). The sign of ω may then be used to distinguish the direction of skin-localization, which is towards the left (right) edge if $J_L < J_R$ ($J_L > J_R$). In comparison, the triple criticality is reduced to a single localization transition point and the NHSEs disappear in the Hermitian limit ($J_L = J_R$) [117]. The physics of quasiperiodic AAH model could thus be greatly enriched by nonreciprocal non-Hermitian effects.

In Figs. 1(b)–1(d), we illustrate the phases and transitions of the noninteracting system via computing some relevant quantities, including the ratio of complex eigenenergies ρ_{Im} , the mean IPR_{ave} of IPRs and the winding number ω . These quantities are defined below. Let us denote the total number of energy eigenstates by D and the number of states whose eigenenergies have nonzero imaginary parts by D_{Im} . The ρ_{Im} is then given by

$$\rho_{\text{Im}} = D_{\text{Im}}/D. \quad (3)$$

When $\rho_{\text{Im}} = 0$ ($\rho_{\text{Im}} > 0$), the system resides in the PT invariant (PT broken) region with a real (complex) spectrum. These two regions are separated by the solid line in Fig. 1(b), which satisfies the phase boundary condition Eq. (2) of the noninteracting \hat{H}_0 . Let $|\psi_j\rangle$ be the j th right eigenstate of the system's Hamiltonian with energy E_j ($j = 1, \dots, D$). We denote the overlap between $|\psi_j\rangle$ and the n th Fock basis by $\psi_n^{(j)}$ ($n = 1, \dots, D$). The IPR of $|\psi_j\rangle$ is then given by

$$\text{IPR}_j = \sum_{n=1}^D |\psi_n^{(j)}|^4 / \left(\sum_{n=1}^D |\psi_n^{(j)}|^2 \right)^2. \quad (4)$$

Averaging IPR_j over all the eigenstates $|\psi_j\rangle$ yields

$$\text{IPR}_{\text{ave}} = \frac{1}{D} \sum_{j=1}^D \text{IPR}_j. \quad (5)$$

Note in passing that we only use right eigenvectors and their standard normalization convention in the calculation of IPR. The IPR of each eigenstate then takes values in the range $[0, 1]$. In the limit of large system size $L \rightarrow \infty$, we have $\text{IPR}_{\text{ave}} \rightarrow 0$ if all the eigenstates $|\psi_j\rangle$ are spatially extended, since the IPR of each state goes to zero as $1/L$ in this case. On the other hand, if a significant portion ($\propto D$) of the eigenstates are localized, the IPR_{ave} would take a finite value, as the IPR of each localized state is finite in the limit $L \rightarrow \infty$. In Fig. 1(c), we find a clear boundary between the regions with vanishing and finite IPR_{ave} , which is given by Eq. (2) for the noninteracting \hat{H}_0 . The same boundary can be identified by evaluating the maximum and minimum of IPRs, which confirms that Eq. (2) indeed describes the critical line of localization transition in the quasiperiodic nonreciprocal AAH model. Finally, the winding number ω counts the number of times that the spectrum of the system winds

around a base point E_0^{B} on the complex energy plane. For the noninteracting \hat{H}_0 , it can be expressed as

$$\omega = \int_0^{2\pi} \frac{d\phi}{2\pi i} \partial_\phi \ln \{ \det [\hat{H}_0(\phi/L) - E_0^{\text{B}}] \}. \quad (6)$$

Here, L is the length of lattice and we choose $E_0^{\text{B}} = 0$ in numerical calculations. The phase factor ϕ/L is introduced via adding a synthetic flux ϕ over the system under the PBC and distributing it uniformly across each bond, so that the hopping amplitudes of the chain are modified as $J_L \rightarrow J_L e^{i\phi/L}$ and $J_R \rightarrow J_R e^{-i\phi/L}$. It is clear that we have $\omega = 0$ if the spectrum of the system is real. If the spectrum is complex with a single loop around E_0^{B} , we would have $\omega = \pm 1$. These cases are observed in Fig. 1(d). Across the PT and localization transitions [Eq. (2)], ω goes from ± 1 to 0. These transitions are thus topological. Passing through the dotted line in Fig. 1(d), ω goes from -1 to 1, which signifies the change of skin-localization direction between left and right edges of the chain under the OBC. Note in passing that no changes are observed around the same dotted line in Fig. 1(c), which is due to the disappearance of NHSEs and skin-localizations under the PBC.

To sum up, nonreciprocal non-Hermitian effects could extend the localization transition point of quasiperiodic AAH model [at $J_L = V = 1$ in Figs. 1(b)–1(d)] into critical lines, through which the system could undergo PT, localization and topological triple phase transitions under the PBC or reverse its skin-localization direction under the OBC. With interactions, the critical point could further expand into a whole intermediate phase, showing both localized and extended states separated by mobility edges under the PBC and skin-localized doublons under the OBC, as will be shown in the following section. Before that, we introduce our tools to characterize the phases and transitions of two interacting bosons.

B. Methods

With interactions, we could also identify the spectral transition of \hat{H} by the ratio of states whose imaginary part of eigenenergies are nonzero, i.e., the ρ_{Im} in Eq. (3), where $D = \frac{(N+L-1)!}{N!(L-1)!}$ counts the dimension of Fock space with two bosons ($N = 2$) in a lattice of L sites. We would have a real spectrum when $\rho_{\text{Im}} = 0$, a mixed one with both real and complex eigenenergies when $0 < \rho_{\text{Im}} < 1$, and a fully complex spectrum when $\rho_{\text{Im}} \simeq 1$.

In our exact diagonalization calculations, we express the Hamiltonian in Fock space with the occupation number representation $\{|2_l\rangle, l = 1, \dots, L\}$ and $\{|1_l, 1_m\rangle, l, m = 1, \dots, L; l < m\}$. Here, $|2_l\rangle$ ($|1_l, 1_m\rangle$) denotes the Fock basis with two bosons on the same (different) lattice site l (sites l and m). To characterize the localization nature of states in real space, we define the symmetrized position eigenbasis as the union of sets $\{|l, l\rangle\}$

and $\{|l, m\rangle + |m, l\rangle/\sqrt{2}\}$, where $l, m = 1, 2, \dots, L$ and $l \neq m$. Here, $|l, m\rangle \equiv |l\rangle_1 \otimes |m\rangle_2$ is just the direct product state of position eigenbases in the Hilbert spaces of the two bosons. The first and second indices of each ket $|l, m\rangle$ denote the positions of two bosons in the lattice. The transformations between Fock and position bases are given by $|2_l\rangle = |l, l\rangle$ and $|1_l, 1_m\rangle = (|l, m\rangle + |m, l\rangle)/\sqrt{2}$. The IPR and its average in Eqs. (4) and (5) can then be computed with respect to the symmetrized position eigenbasis after exact diagonalization. To figure out the existence of intermediate phases with both extended and localized states, we further introduce the maximum and minimum of IPRs as

$$\text{IPR}_{\max} = \max_{j \in \{1, \dots, D\}} (\text{IPR}_j), \quad (7)$$

$$\text{IPR}_{\min} = \min_{j \in \{1, \dots, D\}} (\text{IPR}_j). \quad (8)$$

In the limit of large system size $L \rightarrow \infty$, we have both $\text{IPR}_{\max} \rightarrow 0$ and $\text{IPR}_{\min} \rightarrow 0$ in the extended phase, $\text{IPR}_{\max} > 0$ and $\text{IPR}_{\min} > 0$ in the localized phase, and only $\text{IPR}_{\min} \rightarrow 0$ in the intermediate mobility edge phase. Collecting the information provided by IPR_{\max} and IPR_{\min} then allows us to distinguish the extended, intermediate and localized phases. We may also use a single quantity ζ to identify the presence of intermediate mobility edge phases, which is given by [118]

$$\zeta = \log_{10}(\text{IPR}_{\text{ave}} \cdot \text{NPR}_{\text{ave}}), \quad (9)$$

where $\text{NPR}_{\text{ave}} \equiv \sum_{j=1}^D \text{IPR}_j^{-1}/(LD)$ is the average of normalized participation ratios. In the limit $L \rightarrow \infty$, the function ζ takes finite values in the intermediate mobility edge phase while approaching $-\infty$ in both extended and localized phases. We could then employ IPR_{\max} , IPR_{\min} and ζ to fully characterize the localization nature of different phases and localization transitions in our system. Note in passing that for better illustrations, our presented values of ζ are shifted and rescaled as $(\zeta - \min(\zeta))/\max(\zeta - \min(\zeta))$, where the $\min(x)$ and $\max(x)$ find the minimum and maximum of x over the considered domain of system parameters in Figs. 3 and 6 of the next section.

To identify the topological signatures of spectral and localization transitions with two interacting bosons, we note that the single winding number in Eq. (6) may not be enough, as the extended-to-intermediate and intermediate-to-localized transitions may possess different phase boundaries. To resolve this issue, we introduce a pair of winding numbers (ω_1, ω_2) , defined versus two different base energies (E_1^B, E_2^B) as

$$\omega_\ell = \int_0^{2\pi} \frac{d\phi}{2\pi i} \partial_\phi \ln\{\det[\hat{H}(\phi/L) - E_\ell^B]\}, \quad \ell = 1, 2, \quad (10)$$

where the parametrization of $\hat{H}(\phi/L)$ from \hat{H} is the same as that of $\hat{H}_0(\phi/L)$ [see the discussion below Eq. (6)]. In numerical calculations, we choose $E_1^B = 0$ and set E_2^B as

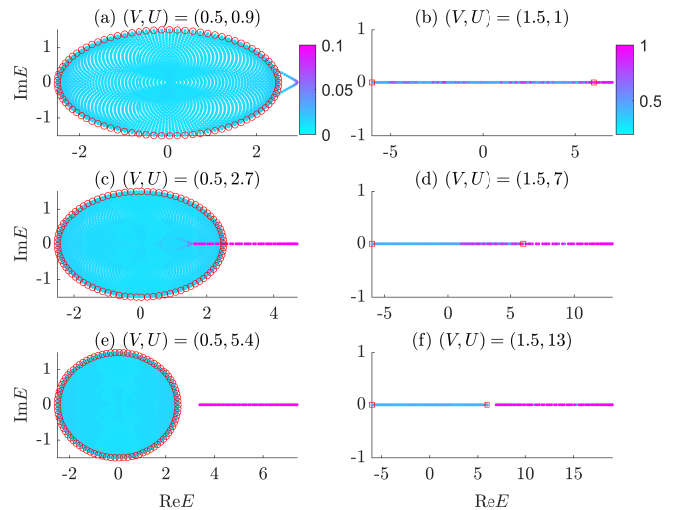


FIG. 2. Energy spectra of the UHM under the PBC. The hopping amplitude is $J = 1$ and the length of lattice is $L = 89$ for all panels. The IPR of each state is given by the color bar. The circles in (a), (c) and (e) denote the spectral boundary E_b [Eq. (13)] of the noninteracting UHM with $V < J$. The squares in (b), (d), and (f) denote the spectral ends $E = \pm 4V$ of the noninteracting UHM with $V > J$. (a), (c) and (e) [(b), (d) and (f)] share the same color bar.

the real part of energy of the eigenstate of \hat{H} with the largest IPR. The quantized change of ω_1 from zero to a finite integer then signifies the transition of the spectrum from real to complex. Meanwhile, the quantized jump of ω_2 from zero to a finite integer corresponds to the delocalization transition, after which all the eigenstates become extended. Therefore, we would have $\omega_1 = \omega_2 = 0$ in a phase with real spectrum and only localized states, $\omega_1, \omega_2 \neq 0$ in a phase with complex spectrum and only extended states, and $\omega_1 \neq 0, \omega_2 = 0$ in an intermediate mobility edge phase with both extended and localized eigenstates. Topological signals of the phase transitions could then be captured by the changes of ω_1 or ω_2 between zero and finite values.

In the next section, we reveal and characterize the interaction induced spectral transitions, localization transitions, and intermediate phases in our system from an integrated perspective of eigenspectrum, state distributions and topology, with the help of the tools introduced in this section.

III. INTERACTION-DRIVEN PHASES AND TRANSITIONS

In this section, we demonstrate the effect of interactions on NHQCs by investigating two representative non-reciprocal hopping models. Their spectral, localization, and topological properties will be treated separately in Secs. III A and III B, with a focus on two interacting bosons. Doublons emerging in strong interaction regions

and their NHSEs will be discussed in the next section.

A. Unidirectional hopping Model (UHM)

We begin our study of the two-body problem with a minimal non-Hermitian AAH model, in which hopping terms along only one spatial direction are kept. Without losing generality, we set $J_L = 0$ and $J_R = J$ in Eq. (1), so that particles can only hop from left to right. The Hamiltonian of this UHM reads

$$\hat{H}_1 = \sum_l \left[J \hat{b}_{l+1}^\dagger \hat{b}_l + 2V \cos(2\pi\alpha l) \hat{n}_l + \frac{U}{2} \hat{n}_l (\hat{n}_l - 1) \right]. \quad (11)$$

In cases with $U = 0$, the spectrum E of \hat{H}_1 with two bosons can be deduced by adding their single-particle eigenenergies [62]. Under the PBC, we would obtain

$$E = \begin{cases} 2V(\cos k + \cos k'), & J \leq V, \\ J(e^{-ik} + e^{-ik'}) + \frac{V^2}{J}(e^{ik} + e^{ik'}), & J > V. \end{cases} \quad (12)$$

Here, k and k' are two synthetic parameters, each filling the domain $[-\pi, \pi)$ densely in the large-size limit $L \rightarrow \infty$. When $J < V$, the spectrum is real with two ending points at $E = \pm 4V$, and all the eigenstates of \hat{H}_1 are localized. When $J > V$, the spectrum is complex with eigenenergies filling an ellipse. Its outer boundary, according to the noninteracting spectrum Eq. (12), is located at

$$E_b = 2Je^{-ik} + 2(V^2/J)e^{ik}, \quad k \in [-\pi, \pi). \quad (13)$$

All the eigenstates of \hat{H}_1 are extended in this case. Thus, a real-complex spectral transition and a localization transition occur together at $J = V$. In the following, we consider the system with two interacting bosons and set $J = 1$ as the unit of energy.

When $U \neq 0$, the spectra in Eq. (12) are modified by the interaction between two bosons. The eigensystem of \hat{H}_1 can then be obtained numerically by exact diagonalization. In Fig. 2, we present the spectra of \hat{H}_1 and the IPRs of the associated eigenstates for some typical cases. We find that for $V < J$, a majority of the eigenenergies are complex and confined within the boundary described by Eq. (13). Meanwhile, with the increase of U , some eigenvalues are first deformed away from the main part of spectrum, forming a small loop around the highest energy of the noninteracting system, and then collapsed onto the $\text{Re}E$ axis. Interestingly, the states with real energies generated by a nonzero U are all spatially localized. We thus obtain an interaction-driven intermediate mobility edge phase, in which extended and localized eigenstates coexist, which is absent in the noninteracting UHM. The further increase of U will generate at most L localized eigenstates with real energies. When U is large enough, their spectrum would finally be gapped from the extended states with complex energies inside E_b . Each eigenstate in the large U regime is formed by a

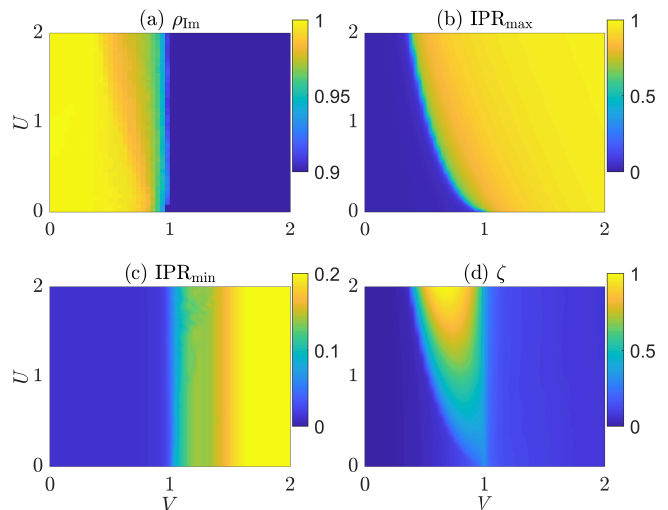


FIG. 3. Spectral and localization transitions of the UHM vs (V, U) under the PBC. The hopping amplitude is $J = 1$ and the length of lattice is $L = 89$ for all panels. (a) Ratio of eigenenergies with nonzero imaginary parts ρ_{Im} [Eq. (3)]. (b) The maximum of IPRs IPR_{max} [Eq. (7)]. (c) The minimum of IPRs IPR_{min} [Eq. (8)]. (d) The smoking-gun function ζ [Eq. (9)] of the intermediate mobility edge phase.

bosonic doublon localized around one lattice site. When $V > J$, the spectrum of \hat{H}_1 retains to be real and all its eigenstates are localized for any nonzero U . This is not hard to expect, as the onsite Bose-Hubbard interaction could only enhance localization, and the localized particles mainly feel the Hermitian quasiperiodic onsite potential $2V \cos(2\pi\alpha l)$. At large U , the spectrum splits into two parts, which are separated by a gap along the $\text{Re}E$ axis. The collection of states with higher energies are again doublons, with each of them containing two bosons localized on the same lattice site.

The above results imply that interactions could transform part of the extended phase of the free-boson UHM into an intermediate one, which contains both extended two-boson states and localized doublons when the interaction is strong enough. To further confirm this, we present the characteristic functions ρ_{Im} [Eq. (3)], IPR_{max} [Eq. (7)], IPR_{min} [Eq. (8)] and ζ [Eq. (9)] of spectra and states over a range of onsite potential and interaction strengths, as shown in Fig. 3. In Fig. 3(a), we observe a complex-to-real spectral transition at $V = J = 1$. The same boundary is found in Fig. 3(c), across which all eigenstates become localized. These observations suggest that the final accomplishment of complex-to-real spectral transition and localization transition are not affected by the onsite Bose-Hubbard interaction in our UHM. However, we notice in Fig. 3(b) a boundary between the regions with $\text{IPR}_{\text{max}} \simeq 0$ and $\text{IPR}_{\text{max}} > 0$, which is different from the boundary $V = J$ of IPR_{min} in Fig. 3(c) while coinciding with the boundary between $\rho_{\text{Im}} \simeq 1$ and $0 < \rho_{\text{Im}} < 1$ in Fig. 3(a). This new phase boundary corresponds to the onset of spectral and localization tran-

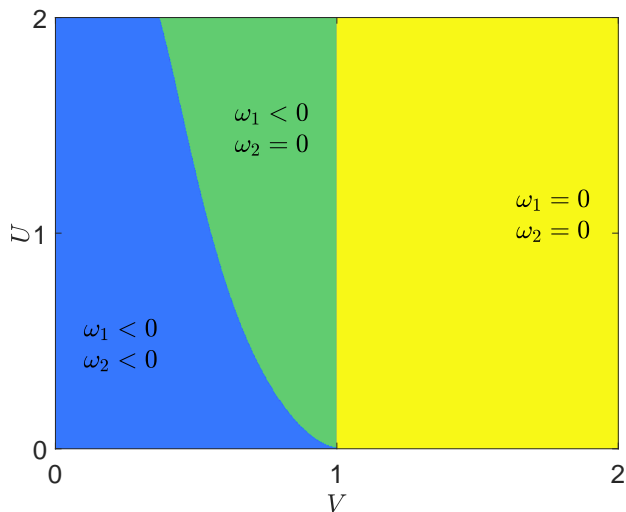


FIG. 4. Phase diagram of the UHM vs (V, U) under the PBC, characterized by the winding numbers (ω_1, ω_2) [Eq. (10)]. The hopping amplitude is $J = 1$ and the length of lattice is $L = 89$.

sitions, which emerges only when $U \neq 0$ and thus has an interaction-origin. However, it could not transform all the states from extended to localized, and the whole spectrum from complex to real. In the region between $V = J$ and the boundary in Fig. 3(b), we now have an intermediate phase with coexisting localized states of real energies and extended states of complex energies. Such a phase is absent without interactions, and its appearance is further confirmed by the function ζ in Fig. 3(d), which shows positive values only in the intermediate mobility edge phase. Putting together, we confirm that interactions in the UHM \hat{H}_1 could indeed generate a mobility edge phase and drive the boundary of extended phase towards the region with weaker disorder strengths.

To decode the topological nature of the observed spectral and localization transitions, we compute the winding numbers (ω_1, ω_2) introduced in Eq. (10), yielding the phase diagram of the UHM in Fig. 4. Within the localized phase, the spectrum of \hat{H}_1 is real and we find $\omega_1 = \omega_2 = 0$, as expected. In the intermediate mobility edge phase, we obtain $\omega_1 < 0$ and $\omega_2 = 0$. The value of ω_1 then undergoes a quantized jump through the real-to-complex spectral transition at $V = J$. In the extended phase, we find both $\omega_1 < 0$ and $\omega_2 < 0$. The value of ω_2 thus experiences a quantized change at the boundary through which all the eigenstates become extended. Therefore, the locations where ω_1 and ω_2 start to deviate from zero in the parameter space could correctly capture all the phase boundaries, offering topological signatures of phase transitions in our system. Note in passing that the exact integer values of ω_1 and ω_2 rely on the times that the corresponding base energies E_1^B and E_2^B are encircled [see Eq. (10)], which could be further dependent on the system size when $\omega_1 \neq 0$ and/or $\omega_2 \neq 0$. For the lattice size $L = 89$ used in our calculations, we find $\omega_2 = -2$ ($= 0$) in the extended (intermediate) phase

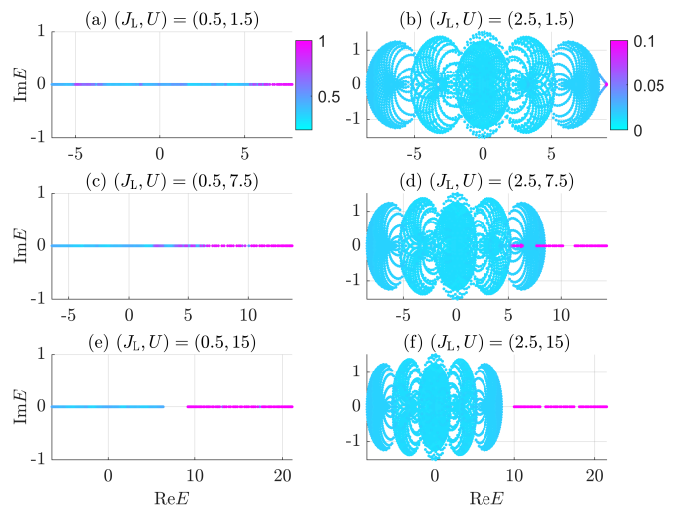


FIG. 5. Energy spectra of the AHM under the PBC. Other system parameters are $(J_R, V) = (1, 1.5)$ and the length of lattice is $L = 89$ for all panels. The IPR of each state is given by the color bar. (a), (c) and (e) [(b), (d) and (f)] share the same color bar.

and $\omega_1 = -27$ in the extended/intermediate phase, respectively. Therefore, the winding numbers (ω_1, ω_2) are expected to provide topological signatures of phase transitions in our system, rather than topological characterizations of the phases with different spectral and localization properties.

To sum up, we find that in the UHM, the interaction between two bosons could enlarge the critical point of the noninteracting system at $V = J$ to an intermediate mobility edge phase, possessing both extended and localized two-boson states with complex and real energies, respectively. The transition from localized to intermediate phases also accompanies a real-to-complex spectral transition, while the transition to extended phase is moved up to the domain with weaker disorder in the presence of interactions. In Sec. III B, we consider the impact of interactions on the more general AAH NHQC with asymmetric hopping amplitudes.

B. Asymmetric hopping model (AHM)

We now go back the original AHM in Eq. (1), treating the case with $J_L, J_R \neq 0$ and $J_L \neq J_R$. To have a good comparison with the results of noninteracting model (as discussed in Sec. II A), we set $J_R = 1$ as the unit of energy and let the quasiperiodic potential strength $V = 1.5$ throughout this subsection. In this case, we have a real-to-complex spectral transition and also a localization transition at $J_L = V = 1.5$ when $U = 0$, as shown in Figs. 1(b)–1(d). Meanwhile, even without interactions, simple expressions of the spectra under PBC could not be found in this case [62]. We thus resort to numerical calculations for characterizing the spectra and states of

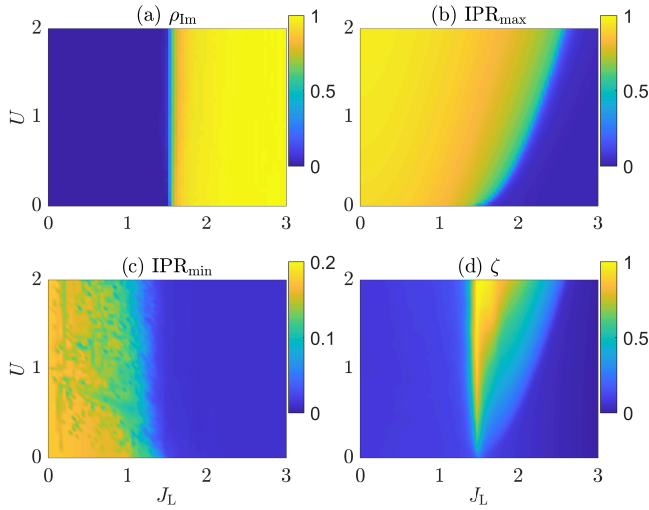


FIG. 6. Spectral and localization transitions of the AHM vs (J_L, U) under the PBC. Other system parameters are $(J_R, V) = (1, 1.5)$ and the length of lattice is $L = 89$ for all panels. (a) Ratio of eigenenergies with nonzero imaginary parts ρ_{Im} [Eq. (3)]. (b) The maximum of IPRs IPR_{max} [Eq. (7)]. (c) The minimum of IPRs IPR_{min} [Eq. (8)]. (d) The smoking-gun function ζ [Eq. (9)] of the intermediate mobility edge phase.

the AHM.

In Fig. 5, we present the spectra of \hat{H} [Eq. (1)] and the IPRs of its eigenstates for typical cases with $U \neq 0$. Qualitatively, we see that the spectral and state features of the UHM are maintained even with nonzero J_L and J_R . Specially, we find that when $J_L < V$, the spectrum of \hat{H} is real and all its eigenstates are localized for $U \neq 0$. Since the onsite interaction only promotes localization, and localized bosons are controlled by the quasiperiodic potential, the spectral properties observed in Figs. 5(a), 5(c) and 5(e) are expected. At large U , the spectrum also divides into two portions gapped along $\text{Re}E$ as that of UHM. The states with higher energies are bosonic doublons localized at different lattice sites. For $J_L > V$, large amounts of eigenenergies become complex. With the rise of U , some energies start to leave the main body of spectrum, composing a loop at the highest energy of the noninteracting AHM, and then pinned to $\text{Re}E$. Similar to UHM, the states with real energies due to a nonzero U are spatially localized. We should then have an interaction-induced intermediate mobility edge phase in the AHM with coexisting extended and localized eigenstates, which disappears when $U = 0$. Further increasing U yields L localized states with real energies. Finally, the spectrum becomes two disconnected sets containing extended states with complex energies and localized bosonic doublons with real energies, respectively. These observations suggest that generic features of the UHM regarding spectral, localization and topological transitions should be carried over to the AHM with both $J_L, J_R \neq 0$.

To gain a more comprehensive understanding, we eval-

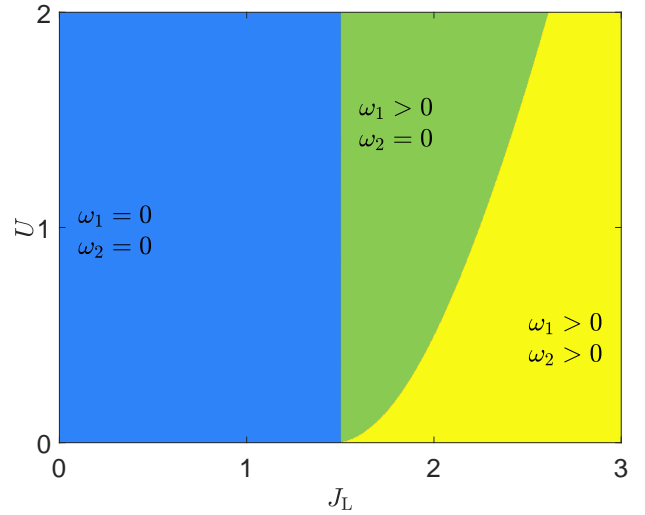


FIG. 7. Phase diagram of the AHM vs (J_L, U) under the PBC, characterized by the winding numbers (ω_1, ω_2) [Eq. (10)]. Other system parameters are $(J_R, V) = (1, 1.5)$ and the length of lattice is $L = 89$.

uate the functions ρ_{Im} [Eq. (3)], IPR_{max} [Eq. (7)], IPR_{min} [Eq. (8)] and ζ [Eq. (9)] in a typical domain of the parameter space (J_L, U) for the AHM, with results presented in Fig. 6. In Fig. 6(a), we realize that the real-to-complex spectral transition of the noninteracting model is essentially not affected by interactions, in the sense that the bulk of eigenenergies turn into complex at any $U \neq 0$ across the transition point $J_L = V = 1.5$ of the $\hat{H}_0 \equiv \hat{H}(U = 0)$ [Eq. (1)]. However, this is not the case for the delocalization transition. In Fig. 6(c), we find that extended states start to appear across the spectral transition at $J_L = V = 1.5$, indicating the onset of delocalization transitions. Nevertheless, the system could enter the extended phase only at a J_L higher than the noninteracting critical point $V = 1.5$ for any $U \neq 0$, as shown by the transition boundary of the IPR_{max} in Fig. 6(b). Therefore, onsite interactions could drive the ending point of delocalization transition of the AHM towards a stronger asymmetric hopping regime. Similar situations have been encountered before in the last subsection, highlighting the generality of local-interaction effects on NHQCs. Altogether, this means that the joint critical point of the spectral and localization transitions of the noninteracting AHM [Eq. (1)] would be split and extended into an intermediate mobility edge phase, carrying both extended states of complex energies and localized states of real energies, with two such examples shown in Figs. 5(d) and 5(f). The presence of such an intermediate phase is further affirmed by the smoking-gun function ζ in Fig. 6(d), which shows finite values only in the region between $J_L = V = 1.5$ [the left boundary of ρ_{Im} and IPR_{min}] and the right boundary of IPR_{max} , i.e., a region sandwiched between the extended and localized phases.

Finally, we check the winding numbers (ω_1, ω_2) in

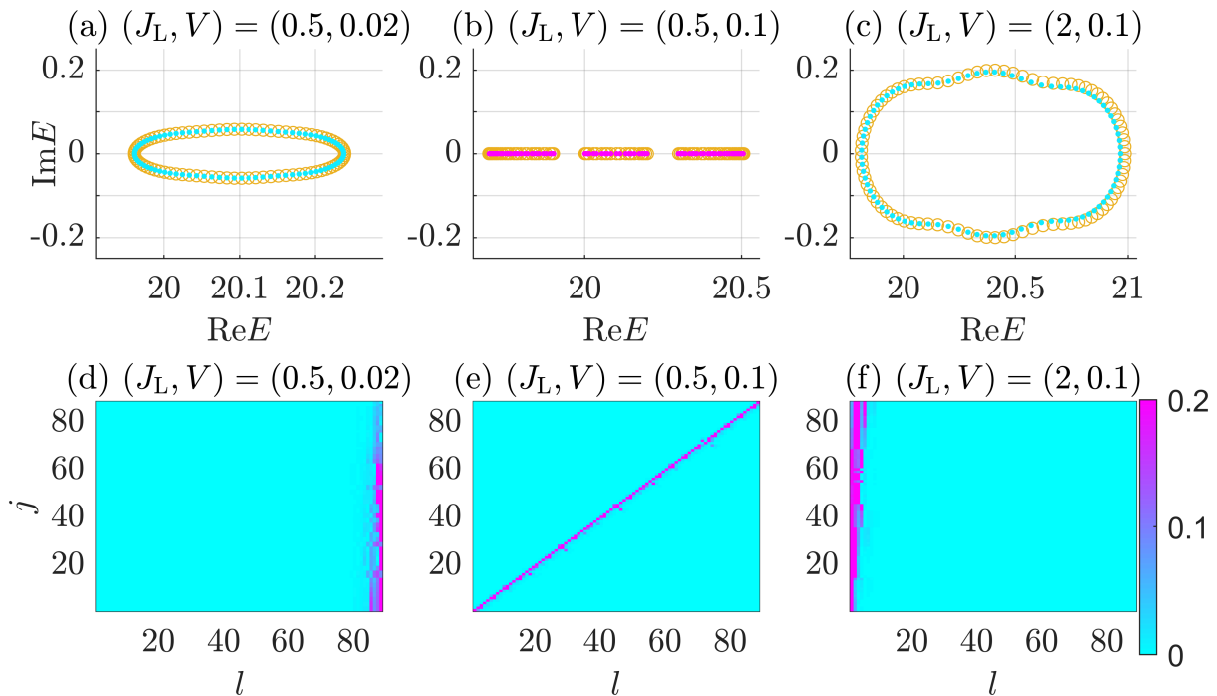


FIG. 8. Energy spectra, IPRs and probability distributions of the bosonic doublons. The length of lattice $L = 89$ and the system parameters $(J_R, U) = (1, 20)$ are taken for all panels. (a)–(f) share the same color bar. In (a)–(c), the dots and circles represent the spectra of \hat{H} [Eq. (1)] in its high-energy sectors and the spectra of $2\hat{H}_2 + U + 4J_L J_R/U$ [Eq. (15)] under the PBC. The colors of dots in (a)–(c) give the IPRs of the corresponding states. (d)–(f) show the probability distributions (measured by the color bar) of all the eigenstates $|\psi_j\rangle$ of \hat{H}_2 under the OBC, with the horizontal and vertical axes representing the lattice and state indices l and j , respectively.

Eq. (10) for the AHM, with results presented in Fig. 7. In the localized phase (with $0 \leq J_L < 1.5$ at any U), the spectrum of AHM is real with no loops on the complex plane, and we find $\omega_1 = \omega_2 = 0$. In the intermediate phase, complex energy loops start to appear in the spectrum, and we find $\omega_1 > 0$ yet $\omega_2 = 0$. The change of ω_1 from zero to a finite integer thus provides the topological signature for the transition from localized to intermediate phases. In the extended phase, we find both $\omega_1 > 0$ and $\omega_2 > 0$. Therefore, the jump of ω_2 from zero to a finite integer offers the topological signal for the transition from intermediate to extended phases. The combination of information provided by ω_1 and ω_2 then allows us to have a complete topological characterization of the spectral and localization transitions in the AHM, which is also consistent with the description based on other quantities in Fig. 6. Note in passing that the signs of winding numbers (ω_1, ω_2) here are different from those of the UHM in the last subsection. The underlying reason is that in the extended and intermediate phases, the skin-localization directions of bulk states in the UHM and AHM are opposite. Under the OBC, the eigenstates are localized at the right edge in the extended and intermediate phases of the UHM, while they are localized at the left edge in these phases of the AHM for our considered parameter space.

To sum up, in two typical nonreciprocal AAH qua-

sicrystals, the cooperation among disorder, interaction and non-Hermitian effects could indeed create unique types of spectral, localization and topological transitions. A key role of the onsite interaction is to dissolve the joint critical point of single-particle spectral and localization transitions and transform it into an intermediate mobility edge phase with both extended and localized states. In the strong-interaction regime, this intermediate phase is expected to hold two disconnected clusters of states. One of them contains extended two-body states, whose spectrum looks similar to the associated noninteracting system. The other one consists of bounded boson pairs forming doublons. We explore the spectral, localization and topological physics of these bosonic doublons in the next section.

IV. DOUBLON PHYSICS

In the Hamiltonian \hat{H} [Eq. (1)] of AHM, if the interaction strength $U \gg (J_L, J_R, V)$, one may treat the noninteracting part $\hat{H}_0 \equiv \hat{H}(U = 0)$ as a perturbation to the Bose-Hubbard interaction term $\hat{H}_{\text{int}} \equiv \sum_l \frac{U}{2} \hat{n}_l (\hat{n}_l - 1)$. In the Fock space of two bosons, the \hat{H}_{int} has two sets of eigenstates, with each of them being highly degenerate. The first set $\{|2_l\rangle | l = 1, \dots, L\}$ has two bosons

on the same lattice site l with the interaction energy $E = U$, which is L -fold degenerate. The second set $\{|1_l, 1_m\rangle | l, m = 1, \dots, L; l < m\}$ has two bosons on different lattice sites with the energy $E = 0$, which is $L(L-1)/2$ -fold degenerate. We can also define projection operators into these two orthogonal subspaces as

$$\begin{aligned}\hat{\mathcal{P}} &= \sum_l |2_l\rangle\langle 2_l|, \\ \hat{\mathcal{Q}} &= \sum_{l,m,l < m} \frac{1}{U} |1_l, 1_m\rangle\langle 1_l, 1_m|. \end{aligned} \quad (14)$$

Using the degenerate perturbation theory up to second order, we could obtain an effective Hamiltonian in the doublon subspace $\{|2_l\rangle | l = 1, \dots, L\}$, which takes the form $\hat{H}_2 = U\hat{\mathcal{P}} + \hat{\mathcal{P}}\hat{H}_0\hat{\mathcal{P}} + \hat{\mathcal{P}}\hat{H}_0\hat{\mathcal{Q}}\hat{H}_0\hat{\mathcal{P}}$ [119, 120]. Working out the \hat{H}_2 for our AHM, we find (up to a uniform onsite energy shift $U + 4J_L J_R/U$ and a global multiplication factor 2) that

$$\begin{aligned}\hat{H}_2 &= \sum_l \frac{1}{U} (J_L^2 |2_l\rangle\langle 2_{l+1}| + J_R^2 |2_{l+1}\rangle\langle 2_l|) \\ &+ \sum_l 2V \cos(2\pi\alpha l) |2_l\rangle\langle 2_l|. \end{aligned} \quad (15)$$

We see that the hopping amplitudes of this doublon effective Hamiltonian is nonreciprocal whenever $J_L^2 \neq J_R^2$, which means that the doublons may also subject to NHSEs under the OBC. Under the PBC, the competition between quasiperiodic potential and asymmetric hopping may further lead to spectral, localization and topological transitions in the doublon subspace at

$$|V| = \max(J_L^2, J_R^2)/U. \quad (16)$$

Interestingly, this condition is different from the critical point [Eq. (2)] of the noninteracting model. Interactions could thus make the bosonic doublons to have different transition thresholds than the noninteracting system.

In Fig. 8, we present spectral and state profiles of the doublons in three typical cases. First, we notice that with $U \gg (J_L, J_R, V)$, the high-energy sectors of the spectra of \hat{H} [Eq. (1)], as denoted by the dots in Figs. 8(a)–(c), could indeed be well approximated by the spectra of the doublon effective Hamiltonian \hat{H}_2 [Eq. (15)], which are given by the circles in the corresponding figures. Second, the spectra of the doublon sectors could either be real or complex. Specially, when $|V|$ is smaller than J_L^2/U or J_R^2/U , the spectrum is complex and form loops on the complex plane, as shown in Figs. 8(a) and 8(c). When $|V|$ is larger than both J_L^2/U and J_R^2/U , the spectrum is real as shown in Fig. 8(b). The condition of spectral transition in Eq. (16) is thus verified. Third, in the situation with a real (complex) spectrum in the high-energy sector, all the eigenstates of the AHM are localized (extended). The Eq. (16) is thus expected to also describe the critical point of localization transition

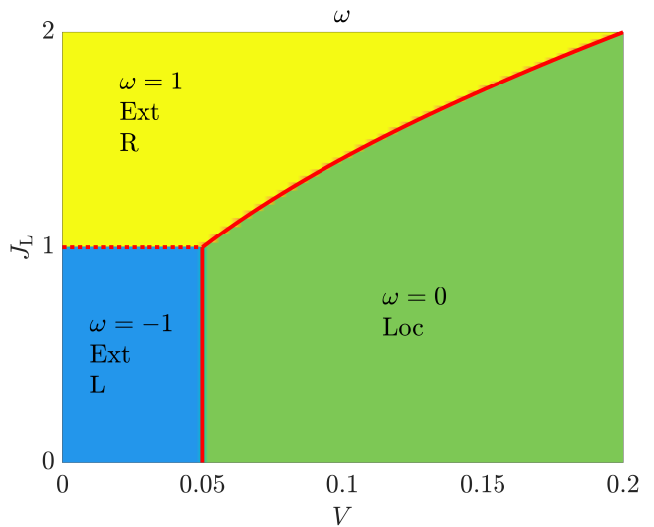


FIG. 9. Phase diagram of the doublon effective Hamiltonian \hat{H}_2 , depicted by the winding number ω [Eq. (6)]. Other system parameters are $(J_R, U) = (1, 20)$ and the length of lattice is $L = 89$. Regions with different colors represent different phases. “Loc” (“Ext”) refers to the localized (extended) phase. “L” (“R”) means that all the bulk states are skin-localized at the left (right) edge of the lattice under the OBC.

for doublons. Finally, we realize that under the OBC, all the doublon eigenstates of \hat{H}_2 become skin-localized at the right (left) edge of the lattice when $J_L^2 < J_R^2$ ($J_L^2 > J_R^2$) and $|V| < \max(J_L^2, J_R^2)/U$, as shown by their probability distributions in Fig. 8(d) (Fig. 8(f)). Therefore, by tuning the relative strengths of hopping J_L and J_R , one could induce NHSEs of doublons, reversing their skin-localization directions, and achieving pumping of doublons from one to the other edge. Meanwhile, if $|V| > \max(J_L^2, J_R^2)/U$, the doublon states are all constituted by strongly bounded boson pairs pinning at different lattice sites, as illustrated in Fig. 8(e). In the AHM, one could then encounter the transition of doublon states between skin-localizations triggered by non-Hermitian effects and Anderson-localizations induced by quasiperiodic potentials, which is unique to interacting and disordered non-Hermitian systems.

To complete our discussion, we show in Fig. 9 the phase diagram of the doublon effective Hamiltonian \hat{H}_2 , which is obtained by computing the topological winding number ω in Eq. (6). Via synthesizing the spectral, localization and topological aspects, we identify three phases for doublons. Their phase boundaries are given by the Eq. (16) (the solid line) and the condition $|J_L| = |J_R|$ (the dotted line) in Fig. 9. When $|V| > \max(J_L^2, J_R^2)/U$, the doublons all form tightly bounded boson pairs with a real spectrum, and they reside in a localized phase with the winding number $\omega = 0$. When $|V| < \max(J_L^2, J_R^2)/U$ and $|J_L| < |J_R|$, the doublon states have complex eigenenergies under the PBC, and they form an extended phase with the winding number $\omega = -1$. Under the OBC, the doublons instead become skin-localized around the

right edge of the system. When $|V| < \max(J_L^2, J_R^2)/U$ and $|J_L| > |J_R|$, the doublon states also possess complex energies under the PBC and constituting an extended phase with the winding number $\omega = 1$. Under the OBC, the doublons are now skin-localized at the left edge of the lattice. Note in passing that the doublon phase diagram at large U in Fig. 9 looks formally similar to the noninteracting single-particle phase diagram at $U = 0$ in Fig. 1(d), even though the state compositions of these two cases are rather different. Overall, the doublon physics discussed here provides another clear evidence for the fact that interparticle interactions could greatly enrich the phase structure of NHQCs.

V. CONCLUSION

In this study, we uncovered rich spectral and localization phenomena driven by the interplay among non-reciprocal hopping, correlated disorder and interparticle interactions in a representative class of non-Hermitian quasicrystal. With a focus on two bosons subject to Hubbard onsite interactions in AAH-type lattices, we revealed that interactions could enhance localization, specially pushing the threshold of localization transition towards stronger hopping regions. Moreover, interactions could give rise to an intermediate mobility edge phase, in which extended two-body states and bounded boson pairs are coexistent. Meanwhile, the transitions between extended, intermediate and localized phases in our system are topological in nature and characterized by a pair of integer quantized winding numbers. Finally, we analyzed the doublon states under strong interactions and unveiled their non-Hermitian skin effects, whose direction could be further controlled flexibly via tuning the asymmetric hopping parameters.

With more than two interacting bosons, there could also be interaction-induced bound states. Intermediate mobility edge phases are thus expected to emerge with the increase of disorder or interaction strengths. For ex-

ample, our preliminary calculations with three interacting bosons yield an intermediate phase, in which localized triplons (three-boson bound states) coexist with extended states. They are also subject to NHSEs under the OBC. In the strong interaction regime, as the effective hopping amplitude of triplons is proportional to $J_{L,R}^2/U$, they will be first localized with the increase of disorder, leading to the localization transition at weaker disorder strengths compared to the noninteracting case. Therefore, although we focus on the case of two interacting bosons in this study, the physical mechanisms underlying the interaction-induced intermediate phases and the NHSEs of multiparticle bound states we revealed are expected to hold in the cases of more than two particles.

In future work, it would be interesting to explore transitions caused by the interplay among non-Hermiticity, disorder, and many-body interactions in higher spatial dimensions. For example, the AAH model can be mapped onto the two-dimensional Hofstadter model, thereby exhibiting fractal spectra and critical eigenmodes [121, 122]. Our preliminary calculations suggest that a Hofstadter “double-butterfly” spectrum could appear in the non-Hermitian AAH model with two interacting bosons. The impact of interactions and non-Hermitian effects on the butterfly spectrum deserves further exploration. In non-Hermitian systems with quasiperiodic or quenched disorder, various types of entanglement phase transitions have recently been identified [72–74]. The influence of interaction on these intriguing entanglement transitions forms another fascinating direction for future research.

ACKNOWLEDGMENTS

We acknowledge Tian Qian for helpful discussions. L.Z. is supported by the National Natural Science Foundation of China (Grants No. 12275260, No. 12047503, and No. 11905211), the Fundamental Research Funds for the Central Universities (Grant No. 202364008), and the Young Talents Project of Ocean University of China.

-
- [1] P. W. Anderson, Absence of diffusion in certain random lattices, *Phys. Rev.* **109**, 1492 (1958).
 - [2] S. N. Mott, Electrons in glass, *Rev. Mod. Phys.* **50**, 203 (1978).
 - [3] E. Abrahams, P. W. Anderson, D. C. Licciardello, and T. V. Ramakrishnan, Scaling theory of localization: Absence of quantum diffusion in two dimensions, *Phys. Rev. Lett.* **42**, 673 (1979).
 - [4] A. Lagendijk, B. v. Tiggelen, and D. S. Wiersma, Fifty years of anderson localization, *Phys. Today* **62**, 24 (2009).
 - [5] D. Belitz and T. R. Kirkpatrick, The anderson-mott transition, *Rev. Mod. Phys.* **66**, 261 (1994).
 - [6] F. Evers and A. D. Mirlin, Anderson transitions, *Rev. Mod. Phys.* **80**, 1355 (2008).
 - [7] P. W. Anderson, D. Thouless, E. Abrahams, and D. Fisher, New method for a scaling theory of localization, *Phys. Rev. B* **22**, 3519 (1980).
 - [8] S. Fishman, D. Grempel, and R. E. Prange, Chaos, quantum recurrences, and anderson localization, *Phys. Rev. Lett.* **49**, 509 (1982).
 - [9] P. A. Lee and T. V. Ramakrishnan, Disordered electronic systems, *Rev. Mod. Phys.* **57**, 287 (1985).
 - [10] A. Punnoose and A. M. Finkelstein, Metal-insulator transition in disordered two-dimensional electron systems, *Science* **310**, 289 (2005).
 - [11] G. Lemarié, H. Lignier, D. Delande, P. Szriftgiser, and J. C. Garreau, Critical state of the anderson transition: between a metal and an insulator, *Phys. Rev. Lett.* **105**, 090601 (2010).
 - [12] N. F. Mott and E. A. Davis, *Electronic processes in non-crystalline materials* (Oxford University Press, Oxford,

- 2012).
- [13] D. A. Abanin, E. Altman, I. Bloch, and M. Serbyn, Colloquium: Many-body localization, thermalization, and entanglement, *Rev. Mod. Phys.* **91**, 021001 (2019).
- [14] J. Billy, V. Josse, Z. Zuo, A. Bernard, B. Hambrecht, P. Lugan, D. Clément, L. Sanchez-Palencia, P. Bouyer, and A. Aspect, Direct observation of anderson localization of matter waves in a controlled disorder, *Nature* **453**, 891 (2008).
- [15] G. Roati, C. D'Errico, L. Fallani, M. Fattori, C. Fort, M. Zaccanti, G. Modugno, M. Modugno, and M. Inguscio, Anderson localization of a non-interacting bose-einstein condensate, *Nature* **453**, 895 (2008).
- [16] B. Deissler, M. Zaccanti, G. Roati, C. D'Errico, M. Fattori, M. Modugno, G. Modugno, and M. Inguscio, Delocalization of a disordered bosonic system by repulsive interactions, *Nat. Phys.* **6**, 354 (2010).
- [17] M. Schreiber, S. S. Hodgman, P. Bordia, H. P. Lüschen, M. H. Fischer, R. Vosk, E. Altman, U. Schneider, and I. Bloch, Observation of many-body localization of interacting fermions in a quasirandom optical lattice, *Science* **349**, 842 (2015).
- [18] J.-y. Choi, S. Hild, J. Zeiher, P. Schauß, A. Rubio-Abadal, T. Yefsah, V. Khemani, D. A. Huse, I. Bloch, and C. Gross, Exploring the many-body localization transition in two dimensions, *Science* **352**, 1547 (2016).
- [19] E. J. Meier, F. A. An, A. Dauphin, M. Maffei, P. Massignan, T. L. Hughes, and B. Gadway, Observation of the topological anderson insulator in disordered atomic wires, *Science* **362**, 929 (2018).
- [20] C. M. Bender and S. Boettcher, Real spectra in non-hermitian hamiltonians having pt symmetry, *Phys. Rev. Lett.* **80**, 5243 (1998).
- [21] A. Guo, G. J. Salamo, D. Duchesne, R. Morandotti, M. Volatier-Ravat, V. Aimez, G. A. Siviloglou, and D. N. Christodoulides, Observation of pt-symmetry breaking in complex optical potentials, *Phys. Rev. Lett.* **103**, 093902 (2009).
- [22] B. Peng, Ş. K. Özdemir, F. Lei, F. Monifi, M. Gianfreda, G. L. Long, S. Fan, F. Nori, C. M. Bender, and L. Yang, Parity-time-symmetric whispering-gallery microcavities, *Nat. Phys.* **10**, 394 (2014).
- [23] M. V. Berry, Physics of nonhermitian degeneracies, *Czechoslovak journal of physics* **54**, 1039 (2004).
- [24] W. D. Heiss, The physics of exceptional points, *J. Phys. A: Math. Theor.* **45**, 444016 (2012).
- [25] B. Zhen, C. W. Hsu, Y. Igarashi, L. Lu, I. Kaminer, A. Pick, S.-L. Chua, J. D. Joannopoulos, and M. Soljačić, Spawning rings of exceptional points out of dirac cones, *Nature* **525**, 354 (2015).
- [26] K. Ding, G. Ma, M. Xiao, Z. Zhang, and C. T. Chan, Emergence, coalescence, and topological properties of multiple exceptional points and their experimental realization, *Phys. Rev. X* **6**, 021007 (2016).
- [27] B. Midya, H. Zhao, and L. Feng, Non-hermitian photonics promises exceptional topology of light, *Nat. Commun.* **9**, 2674 (2018).
- [28] M.-A. Miri and A. Alu, Exceptional points in optics and photonics, *Science* **363**, eaar7709 (2019).
- [29] S. Yao and Z. Wang, Edge states and topological invariants of non-hermitian systems, *Phys. Rev. Lett.* **121**, 086803 (2018).
- [30] F. K. Kunst, E. Edvardsson, J. C. Budich, and E. J. Bergholtz, Biorthogonal bulk-boundary correspondence in non-hermitian systems, *Phys. Rev. Lett.* **121**, 026808 (2018).
- [31] V. Martinez Alvarez, J. Barrios Vargas, and L. Foa Torres, Non-hermitian robust edge states in one dimension: Anomalous localization and eigenspace condensation at exceptional points, *Phys. Rev. B* **97**, 121401 (2018).
- [32] C. H. Lee and R. Thomale, Anatomy of skin modes and topology in non-hermitian systems, *Phys. Rev. B* **99**, 201103 (2019).
- [33] N. Okuma, K. Kawabata, K. Shiozaki, and M. Sato, Topological origin of non-hermitian skin effects, *Phys. Rev. Lett.* **124**, 086801 (2020).
- [34] Z. Gong, Y. Ashida, K. Kawabata, K. Takasan, S. Higashikawa, and M. Ueda, Topological phases of non-hermitian systems, *Phys. Rev. X* **8**, 031079 (2018).
- [35] H. Shen, B. Zhen, and L. Fu, Topological band theory for non-hermitian hamiltonians, *Phys. Rev. Lett.* **120**, 146402 (2018).
- [36] K. Kawabata, K. Shiozaki, M. Ueda, and M. Sato, Symmetry and topology in non-hermitian physics, *Phys. Rev. X* **9**, 041015 (2019).
- [37] C.-H. Liu, H. Jiang, and S. Chen, Topological classification of non-hermitian systems with reflection symmetry, *Phys. Rev. B* **99**, 125103 (2019).
- [38] K. Kawabata, S. Higashikawa, Z. Gong, Y. Ashida, and M. Ueda, Topological unification of time-reversal and particle-hole symmetries in non-hermitian physics, *Nat. Commun.* **10**, 297 (2019).
- [39] C. C. Wojcik, X.-Q. Sun, T. Bzdušek, and S. Fan, Homotopy characterization of non-hermitian hamiltonians, *Phys. Rev. B* **101**, 205417 (2020).
- [40] K. Shiozaki and S. Ono, Symmetry indicator in non-hermitian systems, *Phys. Rev. B* **104**, 035424 (2021).
- [41] N. Hatano and D. R. Nelson, Localization transitions in non-hermitian quantum mechanics, *Phys. Rev. Lett.* **77**, 570 (1996).
- [42] A. Asatryan, N. Nicorovici, P. Robinson, C. M. de Sterke, and R. McPhedran, Electromagnetic localization in one-dimensional stacks with random loss and gain, *Phys. Rev. B* **54**, 3916 (1996).
- [43] J. Feinberg and A. Zee, Non-hermitian localization and delocalization, *Phys. Rev. E* **59**, 6433 (1999).
- [44] A. Jazaeri and I. I. Satija, Localization transition in incommensurate non-hermitian systems, *Phys. Rev. E* **63**, 036222 (2001).
- [45] A. Basiri, Y. Bromberg, A. Yamilov, H. Cao, and T. Kottos, Light localization induced by a random imaginary refractive index, *Phys. Rev. A* **90**, 043815 (2014).
- [46] C. Mejía-Cortés and M. I. Molina, Interplay of disorder and pt symmetry in one-dimensional optical lattices, *Phys. Rev. A* **91**, 033815 (2015).
- [47] N. Hatano and J. Feinberg, Chebyshev-polynomial expansion of the localization length of hermitian and non-hermitian random chains, *Phys. Rev. E* **94**, 063305 (2016).
- [48] Q.-B. Zeng, S. Chen, and R. Lü, Anderson localization in the non-hermitian aubry-andré-harper model with physical gain and loss, *Phys. Rev. A* **95**, 062118 (2017).
- [49] H. Jiang, L.-J. Lang, C. Yang, S.-L. Zhu, and S. Chen, Interplay of non-hermitian skin effects and anderson localization in nonreciprocal quasiperiodic lattices, *Phys. Rev. B* **100**, 054301 (2019).
- [50] S. Longhi, Topological phase transition in non-hermitian quasicrystals, *Phys. Rev. Lett.* **122**, 237601

- (2019).
- [51] S. Longhi, Metal-insulator phase transition in a non-hermitian aubry-andré-harper model, *Phys. Rev. B* **100**, 125157 (2019).
- [52] Y. Huang and B. Shklovskii, Anderson transition in three-dimensional systems with non-hermitian disorder, *Phys. Rev. B* **101**, 014204 (2020).
- [53] A. Tzortzakakis, K. Makris, and E. Economou, Non-hermitian disorder in two-dimensional optical lattices, *Phys. Rev. B* **101**, 014200 (2020).
- [54] Q.-B. Zeng, Y.-B. Yang, and Y. Xu, Topological phases in non-hermitian aubry-andré-harper models, *Phys. Rev. B* **101**, 020201 (2020).
- [55] K.-M. Kim and M. J. Park, Disorder-driven phase transition in the second-order non-hermitian skin effect, *Phys. Rev. B* **104**, L121101 (2021).
- [56] J. Claes and T. L. Hughes, Skin effect and winding number in disordered non-hermitian systems, *Phys. Rev. B* **103**, L140201 (2021).
- [57] X. Cai, Boundary-dependent self-dualities, winding numbers, and asymmetrical localization in non-hermitian aperiodic one-dimensional models, *Phys. Rev. B* **103**, 014201 (2021).
- [58] L.-Z. Tang, G.-Q. Zhang, L.-F. Zhang, and D.-W. Zhang, Localization and topological transitions in non-hermitian quasiperiodic lattices, *Phys. Rev. A* **103**, 033325 (2021).
- [59] Y. Liu, Q. Zhou, and S. Chen, Localization transition, spectrum structure, and winding numbers for one-dimensional non-hermitian quasicrystals, *Phys. Rev. B* **104**, 024201 (2021).
- [60] X. Cai, Localization and topological phase transitions in non-hermitian aubry-andré-harper models with p-wave pairing, *Phys. Rev. B* **103**, 214202 (2021).
- [61] S. Longhi, Non-hermitian maryland model, *Phys. Rev. B* **103**, 224206 (2021).
- [62] S. Longhi, Phase transitions in a non-hermitian aubry-andré-harper model, *Phys. Rev. B* **103**, 054203 (2021).
- [63] S.-N. Liu, G.-Q. Zhang, L.-Z. Tang, and D.-W. Zhang, Topological anderson insulators induced by random binary disorders, *Phys. Lett. A* **431**, 128004 (2022).
- [64] R. Sarkar, S. S. Hegde, and A. Narayan, Interplay of disorder and point-gap topology: Chiral modes, localization, and non-hermitian anderson skin effect in one dimension, *Phys. Rev. B* **106**, 014207 (2022).
- [65] Q. Lin, T. Li, L. Xiao, K. Wang, W. Yi, and P. Xue, Observation of non-hermitian topological anderson insulator in quantum dynamics, *Nat. Commun.* **13**, 3229 (2022).
- [66] A. P. Acharya, A. Chakrabarty, D. K. Sahu, and S. Datta, Localization, pt symmetry breaking, and topological transitions in non-hermitian quasicrystals, *Phys. Rev. B* **105**, 014202 (2022).
- [67] L. Zhou and Y. Gu, Topological delocalization transitions and mobility edges in the nonreciprocal maryland model, *J. Phys.: Condens. Matter* **34**, 115402 (2022).
- [68] X. Cai, Localization transitions and winding numbers for non-hermitian aubry-andré-harper models with off-diagonal modulations, *Phys. Rev. B* **106**, 214207 (2022).
- [69] L.-M. Chen, Y. Zhou, S. A. Chen, and P. Ye, Quantum entanglement of non-hermitian quasicrystals, *Phys. Rev. B* **105**, L121115 (2022).
- [70] T. Orito and K.-I. Imura, Unusual wave-packet spreading and entanglement dynamics in non-hermitian disordered many-body systems, *Phys. Rev. B* **105**, 024303 (2022).
- [71] T. Orito and K.-I. Imura, Entanglement dynamics in the many-body hatano-nelson model, *Phys. Rev. B* **108**, 214308 (2023).
- [72] K. Li, Z.-C. Liu, and Y. Xu, Disorder-induced entanglement phase transitions in non-hermitian systems with skin effects, arXiv:2305.12342 (2023).
- [73] L. Zhou, Entanglement phase transitions in non-hermitian quasicrystals, *Phys. Rev. B* **109**, 024204 (2024).
- [74] S.-Z. Li, X.-J. Yu, and Z. Li, Emergent entanglement phase transitions in non-hermitian aubry-andré-harper chains, *Phys. Rev. B* **109**, 024306 (2024).
- [75] K. Kawabata and S. Ryu, Nonunitary scaling theory of non-hermitian localization, *Phys. Rev. Lett.* **126**, 166801 (2021).
- [76] X. Luo, T. Ohtsuki, and R. Shindou, Transfer matrix study of the anderson transition in non-hermitian systems, *Phys. Rev. B* **104**, 104203 (2021).
- [77] X. Luo, T. Ohtsuki, and R. Shindou, Universality classes of the anderson transitions driven by non-hermitian disorder, *Phys. Rev. Lett.* **126**, 090402 (2021).
- [78] Z. Chen, K. Kawabata, A. Kulkarni, and S. Ryu, Field theory of non-hermitian disordered systems, arXiv:2411.11878 (2024).
- [79] Q.-B. Zeng and Y. Xu, Winding numbers and generalized mobility edges in non-hermitian systems, *Phys. Rev. Research* **2**, 033052 (2020).
- [80] Y. Liu, X.-P. Jiang, J. Cao, and S. Chen, Non-hermitian mobility edges in one-dimensional quasicrystals with parity-time symmetry, *Phys. Rev. B* **101**, 174205 (2020).
- [81] T. Liu, H. Guo, Y. Pu, and S. Longhi, Generalized aubry-andré self-duality and mobility edges in non-hermitian quasiperiodic lattices, *Phys. Rev. B* **102**, 024205 (2020).
- [82] L. Zhou, Floquet engineering of topological localization transitions and mobility edges in one-dimensional non-hermitian quasicrystals, *Phys. Rev. Research* **3**, 033184 (2021).
- [83] L. Zhou and W. Han, Non-hermitian quasicrystal in dimerized lattices, *Chinese Phys. B* **30**, 100308 (2021).
- [84] Z.-H. Wang, F. Xu, L. Li, D.-H. Xu, and B. Wang, Unconventional real-complex spectral transition and majorana zero modes in nonreciprocal quasicrystals, *Phys. Rev. B* **104**, 174501 (2021).
- [85] Z. Xu, X. Xia, and S. Chen, Non-hermitian aubry-andré model with power-law hopping, *Phys. Rev. B* **104**, 224204 (2021).
- [86] Y. Liu, Y. Wang, X.-J. Liu, Q. Zhou, and S. Chen, Exact mobility edges, pt-symmetry breaking, and skin effect in one-dimensional non-hermitian quasicrystals, *Phys. Rev. B* **103**, 014203 (2021).
- [87] W. Han and L. Zhou, Dimerization-induced mobility edges and multiple reentrant localization transitions in non-hermitian quasicrystals, *Phys. Rev. B* **105**, 054204 (2022).
- [88] Y. Liu, Y. Wang, Z. Zheng, and S. Chen, Exact non-hermitian mobility edges in one-dimensional quasicrystal lattice with exponentially decaying hopping and its dual lattice, *Phys. Rev. B* **103**, 134208 (2021).
- [89] C. Yuce and H. Ramezani, Coexistence of extended and localized states in the one-dimensional non-hermitian

- anderson model, *Phys. Rev. B* **106**, 024202 (2022).
- [90] X. Xia, K. Huang, S. Wang, and X. Li, Exact mobility edges in the non-hermitian t_1 - t_2 model: Theory and possible experimental realizations, *Phys. Rev. B* **105**, 014207 (2022).
- [91] S. Longhi, Non-hermitian topological mobility edges and transport in photonic quantum walks, *Opt. Lett.* **47**, 2951 (2022).
- [92] S. Weidemann, M. Kremer, S. Longhi, and A. Szameit, Topological triple phase transition in non-hermitian floquet quasicrystals, *Nature* **601**, 354 (2022).
- [93] Q. Lin, T. Li, L. Xiao, K. Wang, W. Yi, and P. Xue, Topological phase transitions and mobility edges in non-hermitian quasicrystals, *Phys. Rev. Lett.* **129**, 113601 (2022).
- [94] L. Zhou and W. Han, Driving-induced multiple pt-symmetry breaking transitions and reentrant localization transitions in non-hermitian floquet quasicrystals, *Phys. Rev. B* **106**, 054307 (2022).
- [95] L. Zhou, Non-abelian generalization of non-hermitian quasicrystals: Pt-symmetry breaking, localization, entanglement, and topological transitions, *Phys. Rev. B* **108**, 014202 (2023).
- [96] L. Wang, Z. Wang, and S. Chen, Non-hermitian butterfly spectra in a family of quasiperiodic lattices, *Phys. Rev. B* **110**, L060201 (2024).
- [97] E. Levi, M. Heyl, I. Lesanovsky, and J. P. Garrahan, Robustness of many-body localization in the presence of dissipation, *Phys. Rev. Lett.* **116**, 237203 (2016).
- [98] M. V. Medvedyeva, T. Prosen, and M. Žnidarič, Influence of dephasing on many-body localization, *Phys. Rev. B* **93**, 094205 (2016).
- [99] R. Hamazaki, K. Kawabata, and M. Ueda, Non-hermitian many-body localization, *Phys. Rev. Lett.* **123**, 090603 (2019).
- [100] A. Panda and S. Banerjee, Entanglement in nonequilibrium steady states and many-body localization breakdown in a current-driven system, *Phys. Rev. B* **101**, 184201 (2020).
- [101] L.-J. Zhai, S. Yin, and G.-Y. Huang, Many-body localization in a non-hermitian quasiperiodic system, *Phys. Rev. B* **102**, 064206 (2020).
- [102] Y. Wang, C. Cheng, X.-J. Liu, and D. Yu, Many-body critical phase: extended and nonthermal, *Phys. Rev. Lett.* **126**, 080602 (2021).
- [103] S. Heußen, C. D. White, and G. Refael, Extracting many-body localization lengths with an imaginary vector potential, *Phys. Rev. B* **103**, 064201 (2021).
- [104] K. Suthar, Y.-C. Wang, Y.-P. Huang, H. Jen, and J.-S. You, Non-hermitian many-body localization with open boundaries, *Phys. Rev. B* **106**, 064208 (2022).
- [105] H.-Z. Li, X.-J. Yu, and J.-X. Zhong, Non-hermitian stark many-body localization, *Phys. Rev. A* **108**, 043301 (2023).
- [106] M. Ganguli, Spread complexity in non-hermitian many-body localization transition, arXiv:2411.11347 (2024).
- [107] J. Li, L. Ying, and Z. Yang, Imaginary disorder-induced many-body localization and dynamical jumping, *Phys. Rev. B* **110**, 165101 (2024).
- [108] J. Zhang, D. Braak, and M. Kollar, Bound states in the one-dimensional two-particle hubbard model with an impurity, *Phys. Rev. A* **87**, 023613 (2013).
- [109] M. Di Liberto, A. Recati, I. Carusotto, and C. Menotti, Two-body physics in the su-schrieffer-heeger model, *Phys. Rev. A* **94**, 062704 (2016).
- [110] M. A. Gorlach and A. N. Poddubny, Interaction-induced two-photon edge states in an extended hubbard model realized in a cavity array, *Phys. Rev. A* **95**, 033831 (2017).
- [111] P. M. Azcona and C. Downing, Doublons, topology and interactions in a one-dimensional lattice, *Sci. Rep.* **11**, 12540 (2021).
- [112] M. Mark, S. Flannigan, F. Meinert, J. D’Incao, A. Daley, and H.-C. Nägerl, Interplay between coherent and dissipative dynamics of bosonic doublons in an optical lattice, *Phys. Rev. Research* **2**, 043050 (2020).
- [113] S. Longhi, Phase transitions and bunching of correlated particles in a non-hermitian quasicrystal, *Phys. Rev. B* **108**, 075121 (2023).
- [114] T. Qian, Y. Gu, and L. Zhou, Correlation-induced phase transitions and mobility edges in an interacting non-hermitian quasicrystal, *Phys. Rev. B* **109**, 054204 (2024).
- [115] L. Rassaert, T. Ramos, T. Roscilde, and D. Porras, Emerging non-hermitian topology in a chiral driven-dissipative bose-hubbard model, arXiv:2411.08965 (2024).
- [116] Y. Liu and S. Chen, Fate of two-particle bound states in the continuum in non-hermitian systems, *Phys. Rev. Lett.* **133**, 193001 (2024).
- [117] S. Aubry and G. André, Analyticity breaking and anderson localization in incommensurate lattices, *Ann. Israel Phys. Soc* **3**, 18 (1980).
- [118] X. Li and S. Das Sarma, Mobility edge and intermediate phase in one-dimensional incommensurate lattice potentials, *Phys. Rev. B* **101**, 064203 (2020).
- [119] M. Takahashi, Half-filled hubbard model at low temperature, *J. Phys. C: Solid State Phys.* **10**, 1289 (1977).
- [120] Y. Ke, X. Qin, Y. S. Kivshar, and C. Lee, Multiparticle wannier states and thouless pumping of interacting bosons, *Phys. Rev. A* **95**, 063630 (2017).
- [121] A. Borelli, J. Bellissard, P. Jacquod, and D. L. Shepelyansky, Double butterfly spectrum for two interacting particles in the harper model, *Phys. Rev. Lett.* **77**, 4752 (1996).
- [122] L.-J. Lang, X. Cai, and S. Chen, Edge states and topological phases in one-dimensional optical superlattices, *Phys. Rev. Lett.* **108**, 220401 (2012).